



# Modeling stochastic saline groundwater occurrence in coastal aquifers

Massimiliano Schiavo<sup>a,b</sup>, Nicolò Colombani<sup>c,\*</sup>, Micòl Mastrocicco<sup>d</sup>

<sup>a</sup> Department of Land, Environment, Agriculture and Forestry (TESAF), University of Padova, Via dell'Università 16 - 35020 Legnaro (PD), Italy

<sup>b</sup> Department of Civil and Environmental Engineering (DICA), Politecnico di Milano, Piazza L. Da Vinci 32, 20133, Milano, Italy

<sup>c</sup> Department of Materials, Environmental Sciences and Urban Planning (SIMAU), Marche Polytechnic University, Via Brecce Bianche 12, 60131, Ancona, Italy

<sup>d</sup> Department of Environmental, Biological and Pharmaceutical Sciences and Technologies (DiSTABiF), Campania University "Luigi Vanvitelli", Via A. Vivaldi 43, 81100, Caserta, Italy

## ARTICLE INFO

### Keywords:

Salinization  
Aquifers  
Geostatistics  
Trapped seawater  
Saline wedge

## ABSTRACT

The issue of freshwater salinization in coastal areas has grown in importance with the increase of the demand of groundwater supply and the more frequent droughts. However, the spatial patterns of salinity contamination are not easy to be understood, as well as their numerical modeling is subject to various kinds of uncertainty. This paper offers a robust, flexible, and reliable geostatistical methodology to provide a stochastic assessment of salinity distribution in alluvial coastal areas. The methodology is applied to a coastal aquifer in Campania (Italy), where 83 monitoring wells provided depth-averaged salinity data. A Monte Carlo (MC) framework was implemented to simulate depth-averaged groundwater salinity fields. Both MC stochastic fields and the mean across MC simulations enabled to the delineation of which areas are subject to high salinity. Then, a probabilistic approach was developed setting up salinity thresholds for agricultural use to delineate the areas with unsuitable groundwater for irrigation purposes. Furthermore, steady spatial patterns of saline wedge lengths were unveiled through uncertainty estimates of seawater ingress at the Volturno River mouth. The results were compared versus a calibrated numerical model with remarkable model fit ( $R^2=0.96$ ) and versus an analytical solution, obtaining similar wedge lengths. The results pointed out that the high groundwater salinities found inland (more than 2 km from the coastline) could be ascribed to trapped paleo-seawater rather than to actual seawater intrusion. In fact, the inland high salinities were in correspondence of thick peaty layers, which can store trapped saline waters because of their high porosity and low permeability. Furthermore, these results are consistent with the recognition of depositional environments and the position of ancient lagoon alluvial sediments, located in the same areas where are the highest (simulated) salinity fields. This robust probabilistic approach could be applied to similar alluvial coastal areas to understand spatial patterns of present salinization, to disentangle actual from paleo-seawater intrusion, and more in general to delineate zones with unsuitable salinity for irrigation purposes.

## 1. Introduction

Groundwater salinization in coastal aquifers is a long-term issue in hydrogeology (Custodio, 1988; Bear et al., 1999; Barlow, 2003). But with the increasing water demand due to population growth and the accelerating climatic change that triggered prolonged water crises scattered around the world, the attention on coastal groundwater resources recently peaked. These factors have boosted the research of this topic using different approaches, combining the classical hydrogeological and hydrochemical characterization tools with stable isotopes (Kim et al., 2007; De Montety et al., 2008; Cary et al., 2015; Caschetto et al., 2017), or adding geophysical methods (De Franco et al.,

2009; Rasmussen et al., 2013; Trabelsi et al., 2013; Carol et al., 2021a;), or coupling the investigation with density-dependent flow and transport numerical models (Comte and Banton, 2007; Koukadaki et al., 2007; Meyer et al., 2019). Those methods often provide insight into salinization processes, e.g., distinguishing among actual and paleo seawater intrusion (Delsman et al., 2014; Zhao et al., 2017; Bauer et al., 2022), but they suffer from high-quality datasets need, like high-resolution multi-level samplers, isotopes analyses, or expensive geophysical equipment, rarely available except in small and highly characterized areas. To overcome these common issues, several empirical indices have been formulated in GIS environment to assess the vulnerability of coastal aquifers to salinization (Tomaszkiewicz et al., 2014; Trabelsi

\* Corresponding author.

E-mail address: [n.colombani@univpm.it](mailto:n.colombani@univpm.it) (N. Colombani).

<https://doi.org/10.1016/j.watres.2023.119885>

Received 7 December 2022; Received in revised form 6 February 2023; Accepted 15 March 2023

Available online 20 March 2023

0043-1354/© 2023 The Authors. Published by Elsevier Ltd. This is an open access article under the CC BY license (<http://creativecommons.org/licenses/by/4.0/>).

et al., 2016; Motevalli et al., 2019; Kazakis et al., 2019), even with spatial prediction including climate changes (Klassen and Allen, 2017; Busico et al., 2021). Nevertheless, interpolation among poorly characterized variables like hydraulic conductivity or chloride concentrations may produce large uncertainties in the vulnerability maps. Thus, many of the above-mentioned authors suggest taking particular care during the geostatistical analysis of input variables to estimate salinity concentrations across a given study area. In fact, determining high salinity areas via geostatistical methods is usually simpler than using numerical models to achieve the same result. Whereas the former is much simpler, the latter needs proper boundary conditions, set up, and calibration, which may not be a simple task, but often provide the most robust and reliable methods to estimate and quantify the groundwater salinity distribution (Mastrocicco and Colombani, 2021). The employment of artificial intelligence algorithms in recent years have added a novel approach which use the groundwater quality data (Alagha et al., 2017; Taşan et al., 2022), often referred to as surrogate modeling tools. Artificial intelligence algorithms have shown acceptable performance in simulating complex hydrogeological processes and when scarce data do not allow to build up numerical models (Trichakis et al., 2011). Nevertheless, artificial intelligence algorithms suffer the problem of large uncertainties in the produced maps if the training dataset is not well distributed in space and time. To date, stochastic modelling has been applied to many hydrogeological contexts (Fiori et al., 2015; Banusch et al., 2022; Schiavo et al., 2022), but still encounters large resistance to become a standardized practice (Sanchez-Vila and Fernández-García, 2016). Most of the studies on coastal groundwater salinization approach this issue from the modeling side, while few works frame a geostatistical approach, as recently reviewed by Panagiotou et al. (2022), and those treating the problem from the stochastic viewpoint are still a minority (Pool et al., 2015). For example, Abu Al Naeem et al. (2018) employed a combined geostatistical and hydrogeochemical methodology, to assess the extension and origins of highly salinized areas in Palestine, although without using a stochastic framework. Finally, a recent work of Jamei et al. (2022) has analyzed the salinization of groundwater resources in a multi aquifer system in Bangladesh via hybrid artificial intelligence algorithms complemented with a Monte Carlo approach, but only to avoid parameters overfitting.

The present work aims to exploit further points that previous geostatistical-oriented works on aquifer salinization did not highlight. Here the aim is not only to assess salinization patterns in areas where human and agricultural uses of freshwater resources are relevant, but also to produce simulated salinity fields to approach the problem from a stochastic point of view. In particular, the present work is centered on stochastic modelling of salinity simulated fields upon a sequential methodology, employing sparse groundwater salinity data to assess the probability that a certain area is contaminated by an over-threshold of salinity, and to (certainly) evaluate if this area is connected or not with neighboring ones. This analysis may inform water managers about the spatial source and probable connections of salinity concentrations and to quantitatively estimate the probability of an area of being affected by a certain salinity threshold. In order to fully understand and frame different processes that might be involved in salinization issues, the Volturno River mouth area (Italy) has been selected to test whether stochastic modeling fulfills the aim of: (i) reproducing the saline ingression alongside major rivers or in the proximity of lakes (e.g., Lake Patria); (ii) evaluating the saline wedge intrusion uncertainties at different locations respect to a numerical model and an analytical solution, and (iii) appraising the probable extension of highly salinized areas while seeking for the hydrogeological consistency with geological models and available stratigraphic data. The major novelty of this study is that the proposed stochastic interpolation approach has a fast computing time, a simple setup with respect to any density-dependent numerical model and needs fewer data than the latter, and the results may come up consistent with the widest variety of information sources, from paleo-geological to geological, or to numerical ones. Besides, the

present work aims to propose a simplified but robust framework to be employed in other alluvial coastal areas in the world affected by both actual and paleo seawater intrusion problems.

## 2. Methodology

### 2.1. Available data and study area

The coastal unconfined aquifer to test this methodology is the terminal part of the floodplain belonging to the Volturno River mouth, which is located within the Campania Plain, Southern Italy (Fig. 1). The entire Campania Plain has notable economic and ecological values, due to the presence of many farm activities, touristic structures, and wetland protected zones such as the Variconi oasis. The Volturno River coastal plain is located within a large extensional sedimentary basin that developed during the Quaternary and is still actively subsiding, its margins are set among the western arc of the Southern Apennines and the Eastern Tyrrhenian margin (Matano et al., 2014). The actual geomorphological features are a combination of the late Holocene sedimentary evolution and anthropic interventions like urban settlements expansion, land reclamation works, and intensive agriculture (Busico et al., 2021). The selected study area has a rectangular shape with the major axis oriented along the shoreline, is bordered at North by the Agnena River and at South by the Regi-Lagni reclamation canal and its mean ground elevation ranges from -2.0 to 4.0 m above sea level (a.s.l.). At the center of the area lies the terminal part of the Volturno River, while semipermanent water bodies (lagoons and wetlands) like the Patria Lake (Sacchi et al., 2014) are scattered along the coast. The unconfined coastal aquifer is hosted in actual and paleo dune sandy deposits, crossed by several fluvial paleochannels that are interlayered with silty and peaty lenses (Amorosi et al., 2012). A pro-delta unit, formed by silty clay sediments, is present from -16 to -21 m a.s.l.; it represents the local aquiclude of the unconfined coastal aquifer (Zanchetta et al., 2004) (Fig. 1). The study area corresponds to the area of maximum seawater expansion inland during the last Holocenec deglaciation dated back to 6.5 ky before present (Sacchi et al., 2014). Surface waters and groundwater samples were collected in a sampling campaign in September 2019 on 60 monitoring stations (Fig. 1) and analyzed in the field for salinity measurements using a portable multiparameter probe HI 9828 HANNA instruments. The domain of the numerical model previously developed by Mastrocicco et al. (2019) and here employed to compare the present work's results, is highlighted by a yellow box (panel a).

### 2.2. Groundwater setting, salinization patterns and the link with agricultural practices

Groundwater flowlines orthogonally flow from inland areas toward the coastline, mostly following the path of major rivers and with prevailing pattern of submarine groundwater discharge over seawater intrusion along the whole Campania region (Gaiolini et al., 2022). This consideration highlights the importance of understanding salinization patterns along surface water bodies to assess (i) their possible role in vehiculating seawater intrusion or, conversely, (ii) to highlight areas with hazardous salinity which are connected through the aquifer body with the surface network. The area near to the Volturno River is characterized by slightly saline groundwater inland and in proximity to the coast and by reducing conditions due to presence of peaty lenses (Coriello and Ducci, 2014). Groundwater is characterized by sodium absorption ratio and EC values from medium to extremely high, making most of the coastal groundwater unsuitable for irrigation (Mastrocicco et al., 2021). The vulnerability to the actual seawater intrusion extent has been recently estimated via a weighting and rating method (Busico et al., 2021). Here, the highest vulnerability was clearly found along the entire coastline, but very high vulnerability zones were also found along the terminal branches of Volturno and Agnena rivers, up to 4.0 km from

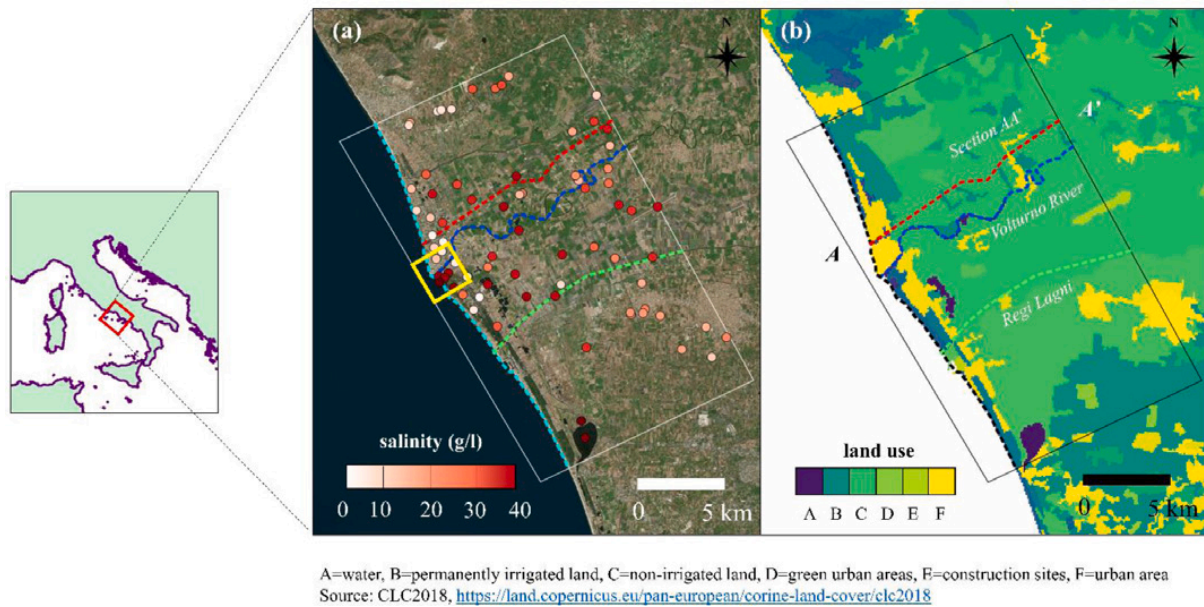


**Fig. 1.** Sketch of the area depicting available borehole data (panel a), with saline contamination values in red gradations, and the land use (panel b). Major rivers (Volturno and Regi Lagni), the coastline and the geological Section AA' (Ruberti et al., 2022) are also highlighted. (For interpretation of the references to colour in this figure legend, the reader is referred to the web version of this article.)

the river mouth. In fact, their riverbeds are located below the Tyrrhenian sea level, possibly promoting seawater encroachment.

### 2.3. Paleolagoon and depositional environments

Recently, Ruberti et al. (2022) have unravelled the paleo reconstruction of the Volturno river coastal plain during the Quaternary. They found that the Volturno coastal plain evolution was driven by sediment supply and global eustatic variations during the Holocene. Briefly, the Mediterranean Sea level rise created a paleo gulf extending up to 10 km inland between 6,5-4,5 ka BP, then a late stage progradation (<4,5 ka BP) was accompanied by the development of a paleo coastal lagoon system that persisted up to the Roman age (Aiello et al., 2018). The associated beach-dune system and coastal lagoons have been relatively stable since the Roman time until early 1800 when a large land reclamation was established and the former Roman Clanio river was channelized and renamed Regi Lagni along with more than 500 km of channels and ditches (Amorosi et al., 2012; Sacchi et al., 2014). The continental depositional facies comprise the Volturno fluvial system, characterized by medium-coarse sand and gravel (paleochannels) passing to silty sand and grey-blue clay (floodplain deposits) and peat (Ruberti et al., 2022). While the bayhead deltaic depositional facies comprise a transgressive barrier, with medium and fine sands interfingering with clay and thick back barrier peaty sediments characterized by high subsidence rates due to presence of peaty lenses and silty clay deposits especially in the area between the Agnena and Volturno rivers (Busico et al., 2021), located in the north-eastern sector of the study area (Fig. 1).

### 2.4. Stochastic modeling of salinity fields

The investigation domain was discretized in squared cells of 0.1 km, for a total amount of approximately  $3 \times 10^5$  cells. Each  $i$ -th cell barycenter is identified by its geographical coordinates  $x_i = (x_i, y_i)$ . Depth-average salinity values were identified by each borehole coordinates  $x_N = (x_N, y_N)$ . A variogram analysis (Goovaerts, 1997; Chiles and Delfiner, 2009) was performed to study the spatial correlation of depth-averaged measured salinity values throughout the domain. This analysis served to model salinity spatial correlation and to simulate a different (random)

value for each  $i$ -th domain site (see Section 3.1). As a first step, the existence of 2D anisotropies was studied by employing directional variograms on the available dataset. Since no preferential directions emerged for data spatial correlation, an omnidirectional variogram model was employed to interpret the spatial distribution of this dataset.

Once this step was achieved, a proper variogram model was calibrated using a best fitting Gaussian function (Deutsch and Journel, 1997) to be used for the simulation of stochastic fields of the variable of interest. Stochastic (conditional) depth-averaged salinity fields rely upon the dataset described in Section 2.1. An isotropic omnidirectional variogram function (Isaaks and Srivastava, 1989) was chosen to interpret the dataset spatial correlation:

$$\gamma(h) = \sigma_N^2 \exp(1 - 3h^2 / a^2) \quad (1)$$

Where  $h = \|x - x'\|$  is the separation distance between vector locations  $x$  and  $x'$  for each  $N$ -th borehole of the dataset;  $\sigma_N^2$  and  $a$  are model parameters, corresponding to the variogram sill and range, respectively. The former was estimated as the variance of the  $N$  available data, while the latter was estimated via a Maximum Likelihood (ML) approach, with best-estimated range of 2.5 km and a 95% confidence interval between lower and upper bounds of 0.3 km.

Then a very well know and widely applied geostatistical methodology, Sequential Gaussian Simulations (SGSIM, Deutsch and Journel, 1997; Remy and Boucher, 2009) was employed to achieve sequential continuous fields of depth-averaged salinity concentration. This enabled to move from the discrete characterization of local salinity that the dataset provided, to the continuous (stochastic) representation of the same variable. Stochastic values are therefore associated with each cell barycenter, embedded by as many as the simulations were performed. Then, the results were collected within a Monte Carlo (MC) framework to be treated as a simulations ensemble.

Three uses of MC salinization fields were performed: (i) considering them one by one as random fields, with locally varying spatial patterns; (ii) thresholding each random field upon one or more salinity values, hence embedding each salinity value as a logical variable (0 or 1) if the prescribed threshold was met or not; and (iii) considering the local mean across simulations ensemble to have the most probable one, since the mean coincides with the most probable value if the spatial distribution



of the latter is gaussian. This moved the analysis toward the domain of probabilities. This can be explained by introducing an indicator variable as follows:

$$I_r(\mathbf{x}_i) = \begin{cases} 1 & \text{if } c_r(\mathbf{x}_i) \geq thr \\ 0 & \text{if } c_r(\mathbf{x}_i) < thr \end{cases} \quad \text{with } r = 1, R \quad (2)$$

$r=1, R$  being each MC simulation,  $c_r(\mathbf{x}_i)$  the local simulated salinity concentration value at the  $i$ -th cell of the  $r$ -th realization, and  $I_r(\mathbf{x}_i)$  is the value of  $I(\mathbf{x}_i)$  in realization  $r$  of the ensemble. Then,  $\chi(\mathbf{x}_i)$  was computed as:

$$\chi(\mathbf{x}_i) = \frac{1}{R} \sum_{r=1}^R I_r(\mathbf{x}_i) = \frac{q}{R} \quad (3)$$

$q$  (an integer between 1 and  $R$ ) being the number of MC simulations where the indicator is equal to one at the  $i$ -th location. Therefore, the indicator  $I(\mathbf{x}_i)$  is a random variable that follows a Bernoulli distribution with probability  $\chi(\mathbf{x}_i)$  given by  $\Pr[I(\mathbf{x}_i) = 1] = \chi(\mathbf{x}_i)$ . Such a probabilistic approach (Schiavo, 2022a) enables to stochastically assess local probabilities of saline concentrations and look for areas most likely to be contaminated.

A geological section (named Section AA' in Fig. 1, already introduced by Ruberti et al., 2022) was employed to appraise the hydrogeological consistency between the MC salinity fields and the conceptualization of the hydrogeological setting of the area. This analysis was extended to additional transects along major rivers (Volturno River and the Regi Lagni canal) and the coastline profile to understand what the probability of a certain salinity does look like.

Analytical solutions for the depth-averaged estimation of the width of the saline wedge inland were employed as reported in Beebe et al. (2016) and references therein. These results were used to verify the consistency of the stochastic saline wedge width along the whole coastline, with a particular interest in the Volturno River mouth (Fig. 1). Here, the MC results were compared with those inferred by a variable density numerical groundwater flow and transport model previously published by Mastrocicco et al. (2019) and performed near the Volturno river mouth within a small portion of the actual study domain. Briefly, the SEAWAT model set up consisted of a squared area of  $1.5 \text{ km}^2$  (yellow square in Fig. 1a) discretized in a regular spaced grid of  $10 \times 10 \text{ m}$  and 12 layers of different thicknesses, enclosing the local ground surface and the top of the prodelta silty-clay unit. Different flow and transport packages were used to fully define the system: the time variant

specified-head boundary package was used to represent the regional freshwater flow boundary and the Tyrrhenian Sea boundary, the river package was employed to simulate the Volturno river, the recharge and the evapotranspiration packages were also used. The SEAWAT model was calibrated versus measured pressure heads and salinities. The squared correlation coefficient  $R^2$  (Taylor, 1997) and the Nash-Sutcliffe Efficiency Index (NSE, Nash and Sutcliffe, 1970) are employed to assess the correlation between the model and present results.

### 3. Results

#### 3.1. Salinity fields Monte Carlo realizations

Stochastic (conditional) salinity fields rely upon the dataset described in Section 2.1 and the variogram modeling described in Section 2.2; a collection of MC realizations of salinity fields was generated as previously described in Section 2.2. A series of 2500 simulations run was necessary to reach the numerical stability of first statistical moments for the simulated salinity at each cell across progressive MC realizations (details not shown). In Fig. 2, exemplary stochastic MC salinity fields are illustrated.

#### 3.2. Salinity agricultural-related thresholds to assess hazardous areas

Two different salinity thresholds (1.5 and 2.5 g/l) have been applied to each MC realization, since most agricultural crops show yield reduction at 1.5 g/l and become substantially affected over 2.5 g/l (Katerji et al., 2003). Each salinity field realization enables to delineate the areas where the employed threshold is exceeded or not. The higher the threshold, the narrower the areas where the threshold is exceeded. Hence, spatial patterns of salinization fields must be investigated if different areas with salinity higher than the prescribed threshold are connected or not. Fig. 3 illustrates the application of the two thresholds to the MC salinity realizations depicted in Fig. 1. The areas with a MC-simulated salinity higher than 1.5 g/l are depicted in light red, while those where the concentration is higher than 2.5 g/l are depicted in red. The areas where salinity concentrations are higher than employed thresholds spread through the outback, being limited to a few clusters of modest width along the coastline zone. Some connections can be assessed if the lower of the two thresholds is employed, being interrupted if the higher threshold is used. This suggests that the inland's high salinity concentrations are clustered in some areas with poor mutual connections between each other and the sea as the main salinity

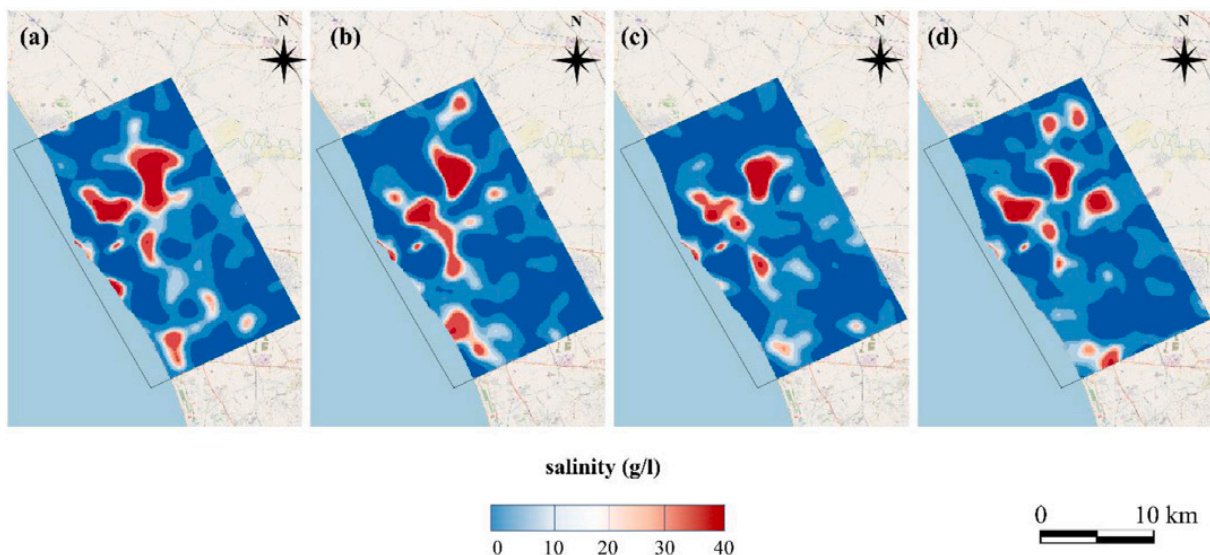


Fig. 2. MC salinity fields realizations for the area of investigation.

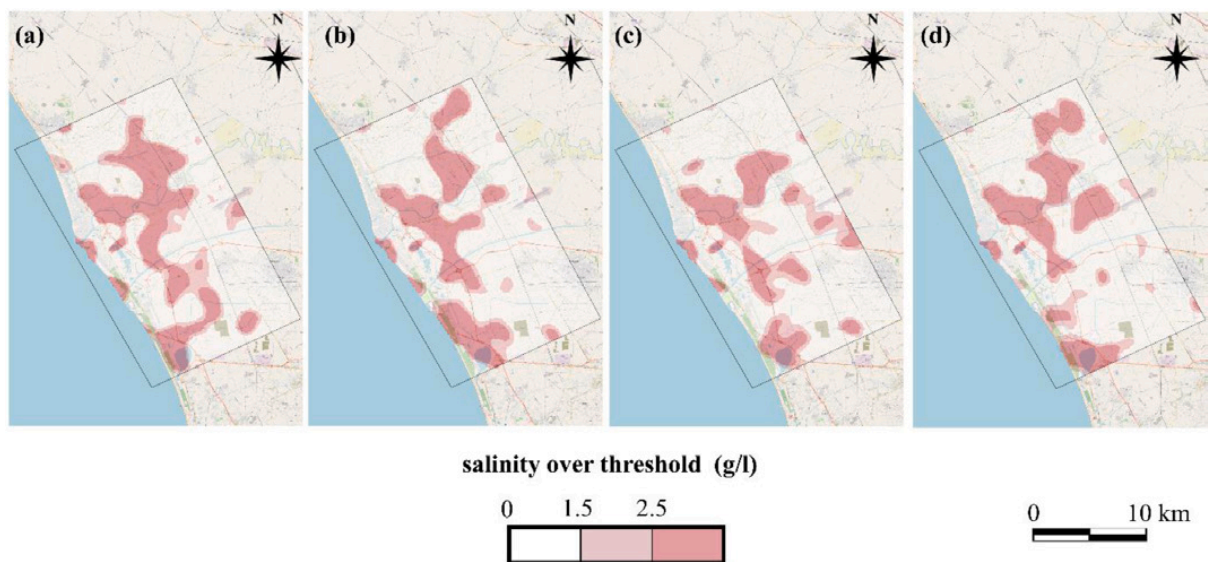


Fig. 3. Thresholded MC salinity fields realizations for the area of investigation.

source. Even such a rough connectivity appraisal may lead to the hypothesis that the Tyrrhenian Sea is the (major) salinity source in the coastline zone, while the inland's source is likely to be different from the actual seawater intrusion.

Ensembling all the MC-salinity fields, the most probable salinity concentration field can be achieved when the mean across each MC realizations is performed at each domain cell. The resulting average salinity field is reported in Fig. 4 (panel a). In panels (b) and (c) of Fig. 4 the probability fields retrieved by employing salinity thresholds of 1.5 and 2.5 g/l are illustrated. As discussed for Fig. 3, the higher the threshold, the narrower are the areas embedded by high  $\chi(\mathbf{x}_i)$  as probability values of exceedance the imposed threshold.

### 3.3. Large-scale geological consistency of salinity and probability fields

A large-scale appraisal of the geological consistency of the stochastic approach here proposed can be assessed through the juxtaposition of an available geological map (Matano et al., 2018) of the area with the mean concentration field (Fig. 4, panel a) and that depicting the probability of having a local concentration higher or equal than 1.5 g/l (Fig. 4, panel b), as illustrated by Fig. 5 in panel a.

Panel b in Fig. 5 enables to appraise which sediment type hosts the highest (average) saline concentration within the study area. Dashed green and magenta lines highlight concentration thresholds of 1.5 and 2.5 g/l (see panels b and c in Fig. 4), respectively. The highest concentration can be assessed where lacustrine peaty and clayey deposits (depicted in light gray blue) are prevalent, while Aeolian ones, located along the coastline, have the lowest concentration. The second sediment

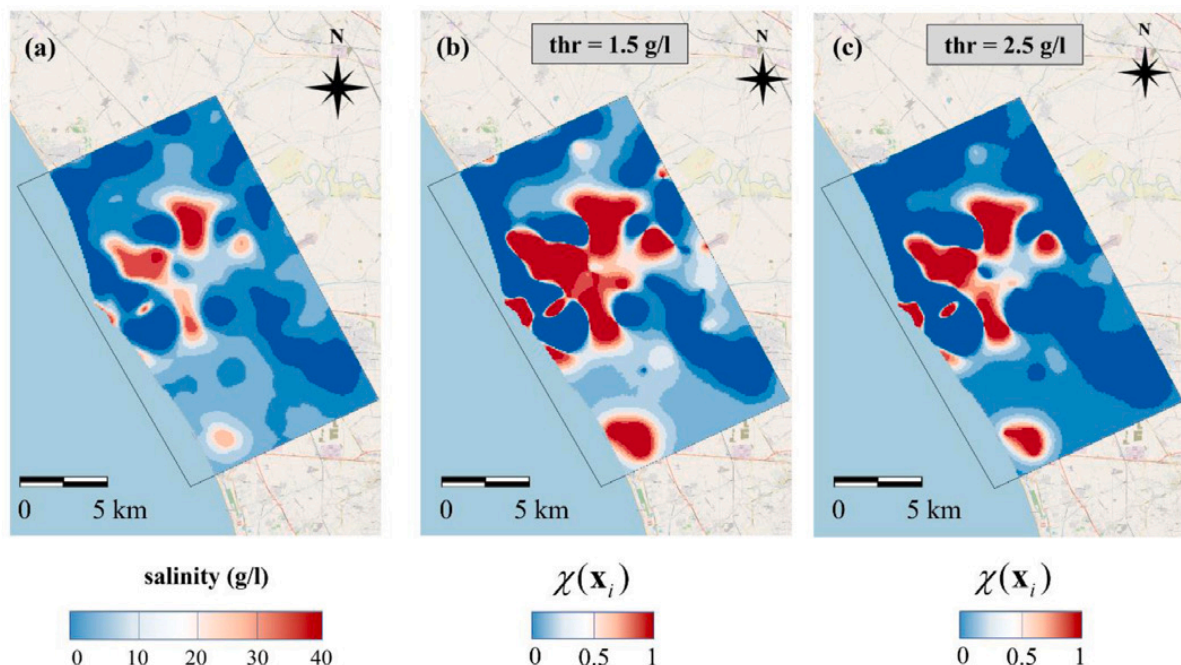
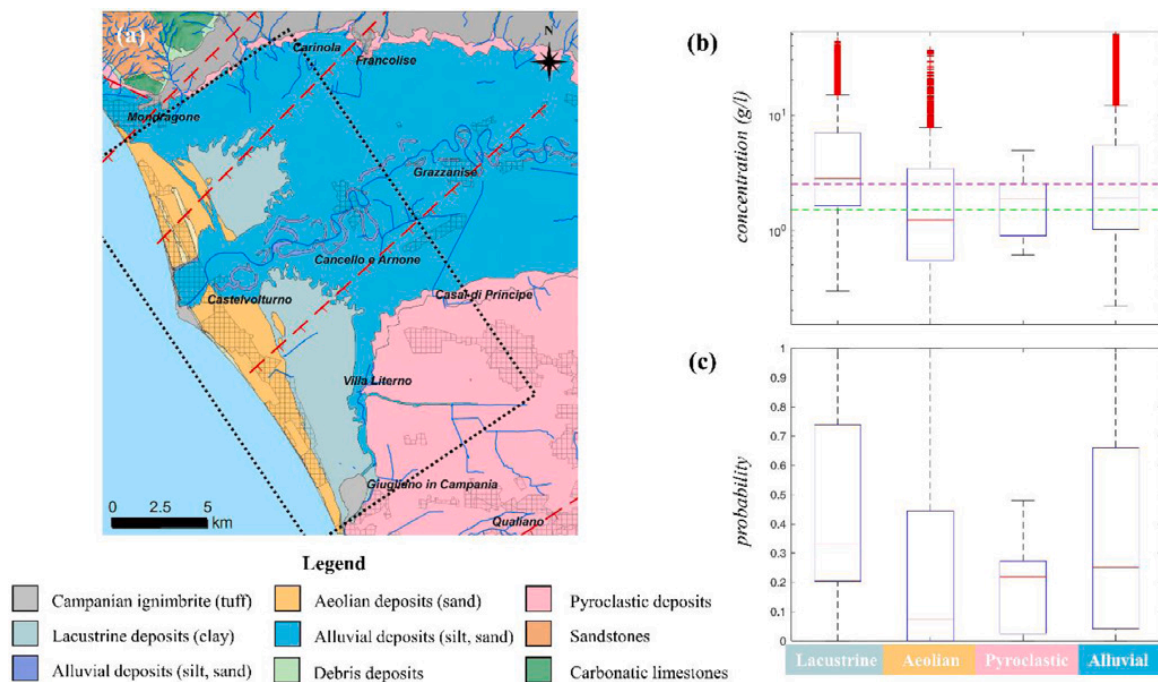


Fig. 4. Average salinity concentration field (panel a), and probability of having a concentration higher than 1.5 and 2.5 g/l (panels b and c, respectively).



**Fig. 5.** Available geological map (panel a), boxplots for saline concentration (panel b) and probability to exceed a local salinity value of 1.5 g/l (panel c) for the main deposits of the area, depicted by colors. Dashed green and magenta lines highlight concentration thresholds of 1.5 and 2.5 g/l (see panels b and c in Fig. 4), respectively. (For interpretation of the references to colour in this figure legend, the reader is referred to the web version of this article.)

facies with the highest salinity concentration are alluvial sediments (depicted in blue), which are a mix of silt, sand, and clay lenses.

Panel c in Fig. 5 enables to correlate the sediment type with the probability of having a saline concentration higher than 1.5 g/l. The highest probability can be assessed where lacustrine peaty and clayey deposits are prevalent (depicted in light gray blue), while sandy permeable Aeolian ones (depicted in light orange), located along the coastline, have the lowest probability of being contaminated by saline concentrations larger than 1.5 g/l. The second sediment facies with the highest probability of being contaminated by concentrations larger than 1.5 g/l are alluvial sediments (depicted in blue), which are a mix of silt, sand, and clay lenses.

### 3.4. Hydrogeological consistency of salinity fields

A more detailed assessment of the salinization in particular areas of the domain can be done if both the concentration and the probability of exceeding a threshold are investigated. Therefore, 4 transects are delineated (see Fig. 1) to be inspected: (i) one along the Volturno River thalweg; (ii) one along the Regi Lagni canal thalweg; (iii) one along the coastline, with the aim of understanding the seawater wedge penetrating inland; and (iv) one along a geological section to inspect for the geological consistency of the salinization spatial fields here proposed. Both panels in Fig. 6 are dedicated to this task. Fig. 6 panels illustrate the average salinity concentration field (from a to d) and the probability  $\chi(x_i)$  (from e to h) of having a local value higher than 1.5 g/l along the Volturno River (panels a and e), the Regi Lagni canal (panels b and f), the coastline (panels c and g), and the geological Section AA' (panels d and h), respectively.

The salinity probability profiles (Fig. 6) indicate elevated salinities in the proximity of the coastline, as one can expect due to actual seawater intrusion. After being mostly neglected moving inland, both the salinity and the probability profiles highlight an abrupt increase at more than 5 km from the coastline. This evidence strengthens the thesis that the high inland salinity concentration does not depend on the salinity of the sea or on the effect of the saline wedge inland penetration, but rather

depends on relict paleo-seawater trapped within highly porous clayey soil layers. This behavior can be appraised also from panels b and f, where the highest salinity and probability values (in the proximity of the sea and 6–7 km inland, respectively) seem to be poorly connected by low counterparts located from 2 to 5 km from the coastline, as well as the probability of high salinity values from 2 to 5 km inland are very low, as one can appraise by comparing the latter panels with panels b and c in Fig. 4.

Furthermore, panels c and g in Fig. 6 reveal that salinity and probability peaks along the coastline are in proximity of major surface water bodies. The three salinity peaks detected from panel c in Fig. 6 can be associated to the Volturno River, Regi Lagni Canal, and Lake Patria (in the southern part of the domain, see Fig. 1), respectively.

The latter water body is well connected to the Tyrrhenian Sea through a cemented channel and is characterized by high salinity. This local salinization pattern is, however, poorly correlated with the surrounding salinity values (see also Fig. 4's panels), suggesting a localized salinity pattern that may not affect the surrounding inland aquifer due to the poor connection of the Patria Lakebed (consisting of silty clay sediments) with the coastal aquifer (Sacchi et al., 2014). Panels d and h in Fig. 6 suggest that the highest salinity values, as well as the highest probabilities of having over-threshold concentrations, are in areas where thick organic clayey layers are identified (Busico et al., 2021; Ruberti et al., 2022), strengthening the idea that inland salinity may be likely to depend on trapped paleo-seawater rather than actual seawater intrusion.

### 3.5. Ancient quaternary lagoon consistency of simulated salinization patterns

The highest values of (simulated) salinity, achieved from the mean across MC-realization of local salinity, are concentrated where the back barrier peaty depositional facies are located; which is consistent with the palaeogeographical evolution of the area depicted in Fig. 7. The nature of these depositional facies rules local circulation patterns within the subsurface, as well as water flow energy dissipation, hence being useful



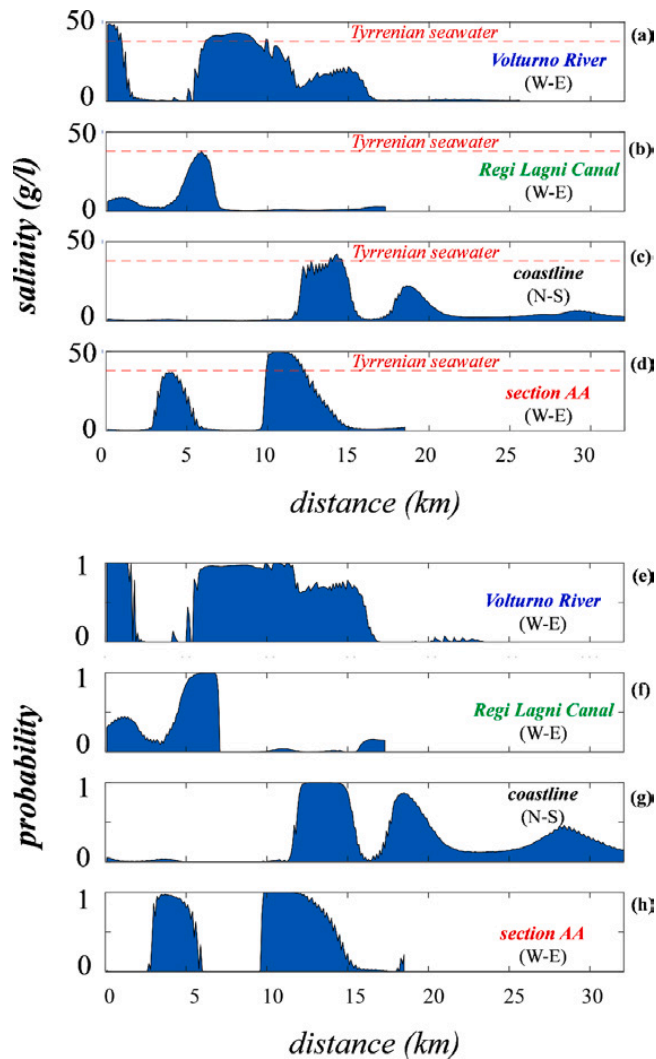


Fig. 6. Salinity concentration and probability of having a salinity value higher than 1.5 g/l along dedicated transects.

to inform about salinization processes.

Other footholds to the proposed thesis can be retrieved if water table measurements, sourced from Gaiolini et al. (2022), are compared with salinization values and divided for different depositional environments. The latter environments are illustrated in Fig. 8 and referring to areas depicted in Fig. 6: Lacustrine, Aeolian, Pyroclastic, and Alluvial sediment areas (in panels a, b, c, and d, respectively).

The highest values of water table are measured within lacustrine or alluvial depositional environments, the lowest where pyroclastic and aeolian sediments are located. Aeolian sediments are well-acknowledged (see e.g. Ruberti et al., 2022) for being in connection with the coastline, as indicated by lower water table levels than their lacustrine counterparts. On the contrary, the lacustrine environment is characterized by water table levels higher than the sea level of 2–3 m (on average), hence being disconnected from the sea. Therefore, the latter one is the most likely to trap paleo-seawater, being geologically (see Section 3.3) and hydrogeologically (see Section 3.4) disconnected by the present seawater intrusion.

### 3.6. Assessing the role of the present seawater from a stochastic point of view

At this point, it is interesting to quantify the inland penetration of the Tyrrhenian Sea to understand its role in the salinization of coastal

aquifers. It is pivotal to assess if the connection with high salinity values far from the coastline may be associated, within a probabilistic framework, to those in the proximity of the Tyrrhenian Sea. This can be done within the present stochastic approach by taking each of the MC realizations and plotting the width of the saline wedge along the Tyrrhenian Sea coastline. The results are illustrated in Fig. 9. In panel a, each of the  $R$ -th realizations corresponds to a blue line, while the mean across these is the red line; the latter informs that the maximum inland saline penetration from the sea occurs at the mouth of the Volturno River, with a mean value of 520 m. This result is confirmed by the application of analytical solutions (Fig. 9, panel b), commonly used for the evaluation of the maximum width of the saline wedge in coastal aquifers (Werner et al., 2013; Beebe et al., 2016), upon hydrogeological data on the aquifer under investigation (Mastrocicco et al., 2021).

The reliability of the present approach can be sustained by comparison with the latest available numerical model, calibrated for a portion of the domain. The mean across the MC salinization fields is correlated with that inferred from a SEAWAT (Langevin et al., 2007) numerical simulation calibrated by Mastrocicco et al. (2019) in an area located at the Volturno River mouth. The comparison performed between the numerical calibrated model and the present work's results are reported in Fig. 10 (panel a), as well as their correlation appraised via  $R^2$  and NSE index coefficient (see Section 2), while statistics regarding the similarity of statistical moments are reported in panel b. The mean across the MC salinity fields slightly overestimated local salinity values, in particular medium ones, returning an overall very good outcome (0.96). An NSE of 0.74 reveals a good consistency between the two models' spatial salinity fields. The ratios of the first statistical moments (with  $\sigma$  as the standard deviation,  $s$  as the skewness, and  $k$  as kurtosis) evaluated between the model (mod subscript) and the average salinity field (MC subscript) are fair enough to give credit to the results here presented. The latter ratios are enough to regard the two populations of local salinity values (i.e., the modeled and the mean across the MC ones) as statistically mutually consistent. The uncertainty related to the approach here employed, as well as the one related to data uncertainty and Kriging parameters (see e.g. Athens and Caers, 2022; Schiavo, 2022b;) should be investigated for a deeper assessment.

### 3.7. Geostatistical variograms

All the proposed results have stemmed from a geostatistical methodology, hence they need to be recovered to the initial viewpoint for a complete process understanding. Fig. 11 depicts experimental variograms retrieved for salinity values (see Fig. 4 and panels therein), measured at wells locations, for 30 (in orange) and 120 (in green) degrees principal directions, along those the domain has been oriented. Each directional variogram shows experimental points within the normal score space (Goovaerts, 1997), with a red dashed line highlighting the experimental variance (hence equal to 1) and a shadowed box highlighting the experimental data range of variation, i.e. the range of (possible) distances needed to reach a lack of spatial correlation between randomly taken points.

Although the present results fully rely upon the usage of an omnidirectional variogram, which is needed to retrieve the spatial variation of the variable of interest for the whole domain without preferential directionalities (Schiavo, 2022a, for an application with the same issue), the inspection of directional variograms may be of interest to understand how salinity varies along principal axes. As Fig. 11 illustrates, the range of lags for reaching the sill along a 30-deg direction is double (about 7 km) that along the 120-deg one (about 3.5 km). While the former rules the variation of salinity fields (hence of the mean across the MC realizations, as illustrated in Fig. 4, panel a) with the domain's width, the latter reproduces that along the coastline or parallel directions. This means that salinity fields varying across the domain's width are far more correlated than those along the coastline, where high values of salinity are present in some hotspots (such as river mouths),

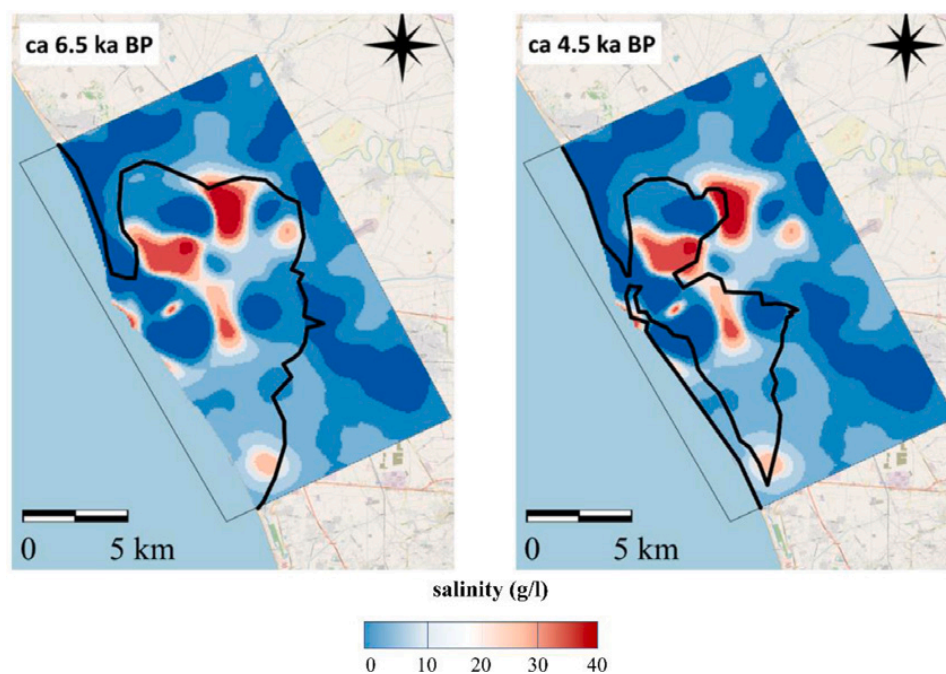


Fig. 7. Average salinity concentration field compared with the paleo gulf shape (panel a) and with the paleo lagoon shape (panel b) from Ruberti et al. (2022).

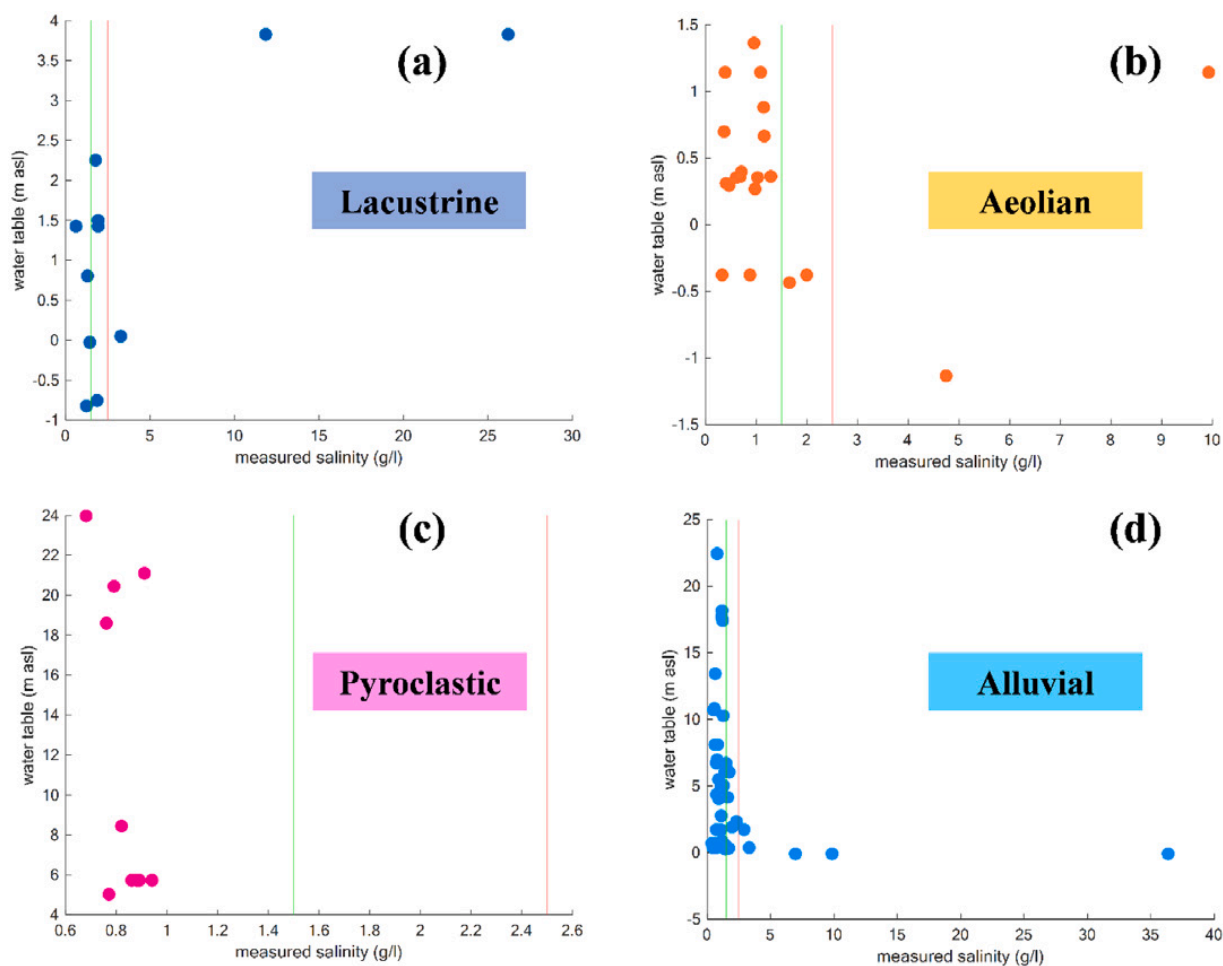
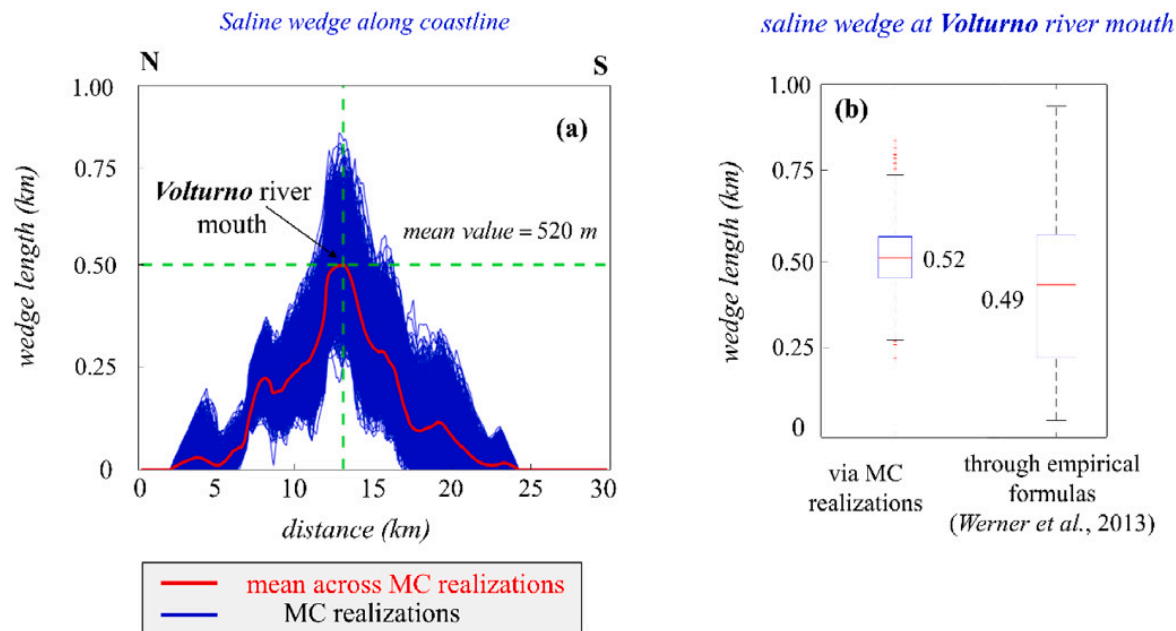
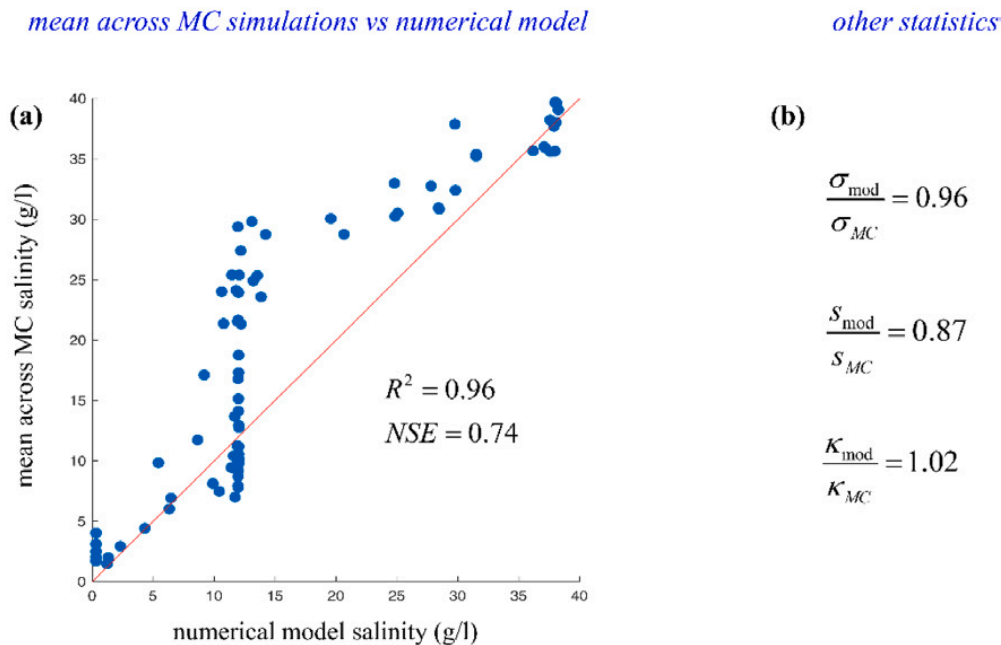


Fig. 8. Scatter plots of measured salinity versus water table elevation from Gaiolini et al. (2022).





**Fig. 9.** Stochastic evaluation of the saline wedge inland penetration along the coastline (a) and the comparison between the MC realizations and empirical formulas (b).



**Fig. 10.** Comparison between the salinity field retrieved from a calibrated numerical model and the mean across the MC ones (a); and the appraisal of the ratios calculated between model vs MC average salinity fields for: standard deviation, skewness, and kurtosis (b).

but highly mutually disconnected (see the sparsity of reddish areas along the coastline in Fig. 4, panel a). Moreover, the variability of experimental points variances (horizontal blue arrows) for the 120-deg direction (green dots) on the sill (vertical black arrows) abruptly changes within narrow distances (twice of the experimental variance), as one may appraise from short-lagged experimental points. Conversely, most of the points within the range of variation of the sill for the 30-deg directional variogram (orange dots) are characterized by lower changes in experimental variances (about a half of the experimental variance), especially for distances between points higher than 2–3 km. Large or narrow changes in experimental variance for experimental variogram points along a certain direction implies an even larger or

narrower (non-linear) variation in local simulated salinity, since local values would disclose to the mean salinity (i.e. embedded with a standard deviation) with the square root of the variance. Short-lagged points are embedded by experimental variances significantly more varying (with the lag) than those located at distances higher than 2–3 km and far less correlated than those. These geostatistical consistency sources are consistent with discontinuous patterns of salinity from the coastline with inland areas, inferred in Section 3.1.

#### 4. Discussion

This work presents a stochastic approach to model saline occurrence

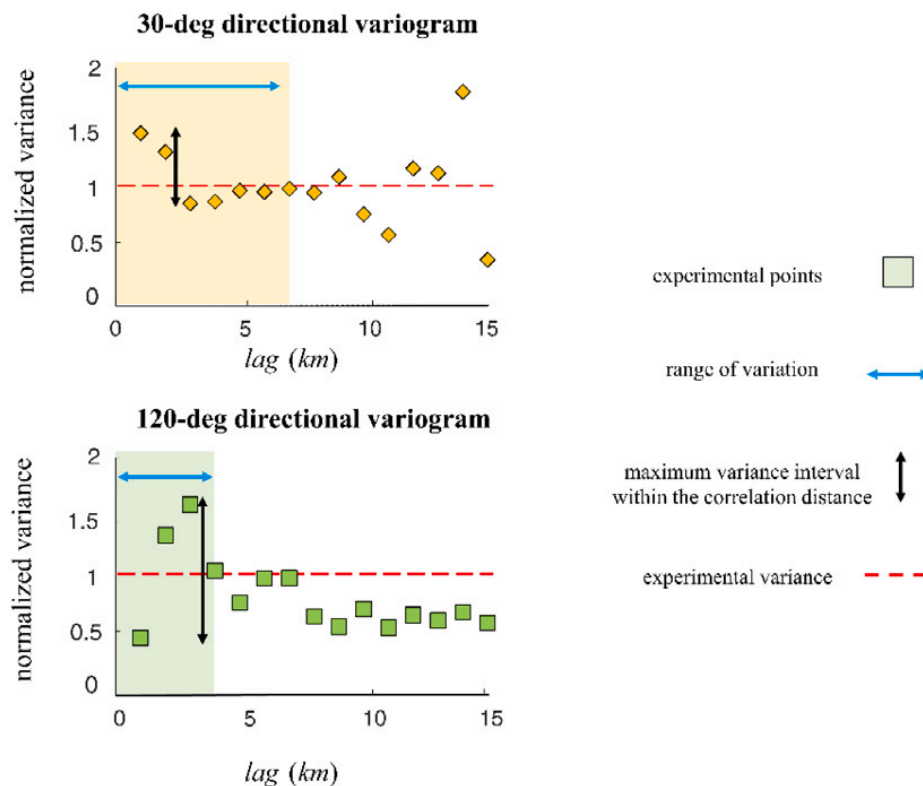


**Fig. 11.** Directional 30-deg and 120-deg mean-across-MC salinity variograms. Their appraisal enables to fully understand how salinization patterns vary along these principal axes.

in coastal alluvial aquifers. The aim of the present work is to frame a complex hydrogeological problem to offer a stochastic approach, a robust geostatistical methodology, and a real case-study application, strengthened by several proofs about the consistency of the employed approach, coming from different sources (geological, hydrogeological, salinization processes-based). This methodology starts from observed depth-averaged salinity concentrations, collected within the Volturno River floodplain area. Grounding on a well-acknowledged geostatistical simulation method, the present approach enables to retrieve Monte Carlo simulations of salinization concentrations in each location of a regularly gridded domain, which is preliminarily considered as bi-dimensional. The numerical results are offered as (i) stochastic salinity fields, (ii) mean concentration fields obtained as the average across the MC ensemble, and (iii) maps with the local probability that the (average) simulated salinity exceeds a threshold value. The importance of uncertain spatial evaluation of salinization areas is fundamental to assess where groundwater resources are suitable for human or agricultural uses (Bierkens and Wada, 2019).

The results shown in Sections 3.1 and 3.2 highlight that the highest salinization values are located (i) along the coastline, suggesting actual seawater intrusion; or (ii) far inland as isolated clusters, embedded by very low probability of being connected with the (present) coastline. The latter salinized areas are the source of most of the concerns, because of the high density of human and agricultural-related activities in the area. The gathered information suggests that these salination clusters depend on paleo-trapped seawater. This thesis is supported by multiple footholds, which can be divided in different groups. Section 3.3 deepens how high inland salinization values are mostly located where lacustrine and alluvial sediments, geologically disconnected by the coastline, are located. Section 3.4 shows the hydrogeological setting of inland salinized areas, which are likely of being disconnected from the coastline along major river body tracks, coastline, and geological sections of interest, suggesting a negligible probability of the interaction of present seawater inland. These analyses are also supported by the fact that, apart from

those located along the coastline, the highest salinized wells are located where the aquifer thickness is enough (at least 25–30 m, within lacustrine or alluvial sedimentary geological zones) to include peaty-clayey lenses, which are highly likely of being able to trap paleo-seawater, as reported and discussed in Section 3.5.

Moreover, the hydraulics of these areas confirm these suggestions, since the highest salinized wells are located where low and spatially constant water table levels are measured, and local hydraulic gradients are very low. In these areas, the local water table levels are however higher than the sea level, hence being clearly hydraulically disconnected from the seawater. Furthermore, salinization patterns appear to be intimately related to different kinds of depositional environments, as reported in Sections 3.3 and 3.5. In addition, a paleo-geological analysis suggest that the ancient lagoon environment is trapping paleo-seawater, responsible for the present inland hazardous salinization, as proposed by previous paleo-geological literature works (see Section 3.6); moreover, a supplementary geostatistical analysis (Section 3.8) supports this by detecting precise spatial patterns, through variograms' directionality analysis, of inland salinization. The same salinization patterns also occur in other areas in the Mediterranean area (Mastrocicco and Colombani, 2021) and worldwide (Wang and Jiao, 2012; Carol et al., 2021b), where groundwater and seawater interface positions are a result of late Quaternary paleoenvironmental conditions, with evaporites dissolution in back barrier environments which creates brines even at shallow depths (Delsman et al., 2014; Liu et al., 2017; Caschetto et al., 2017).

Finally, in Section 3.7 the inland penetration length of the present seawater wedge is estimated of being lower than 0.5 km along the entire coastline, with an expected maximum at the mouth of the major river of the area (Volturno River). These analyses, performed with a stochastic approach, are consistent with analytical solutions which are more commonly used for these purposes and with the latest available numerical models calibrated for the investigated area, supporting the present thesis.

## 5. Conclusions

A stochastic framework has been proposed to investigate coastal aquifers salinization and assess most vulnerable areas. The core of this study is the sequential simulation of salinity fields. The results achieved from simulations' ensemble, treated from a probabilistic perspective, are consistent with previous datasets, a wide variety of consistency sources, and available simulations. Key points of the present work can be summarized as follows:

- (i) Highest salinities are located at the mouth of the main rivers or far inland, the latter as isolated clusters. The probabilistic analysis suggests a different origin for these two salinization phenomena since no probable spatial connection exists between the former and the latter.
- (ii) The study of over-threshold salinities allowed to appraise which areas are more likely of being affected, becoming unsuitable for human freshwater supply or agriculture use.
- (iii) Inland high salinity concentrations are located where relevant peaty layers are framed within the subsurface water bodies. This strengthened the hypothesis that the inland salinities arise from trapped paleo-seawater, rather than from actual seawater intrusion.
- (iv) The stochastic approach enabled to have a reliable appraisal of the inland penetration of the saline wedge along the whole coastline. The highest salinities are confirmed to be expected at the Volturno River mouth, and the actual seawater wedge width does not propagate inland for more than 0.5 km (as average estimation across MC scenarios). This result is consistent with different sources of information: previous literature works, a local calibrated numerical model, and the use of empirical formulas.

These results are consistent with paleo-salinization patterns, retrieved from geological and sedimentary assessment of the areas where lacustrine sediments were deposited with the withdrawal of the ancient lagoon. Furthermore, the recognition of different depositional environments enables to differentiate different magnitude of salinization. The highest values occur in lacustrine-like sediments with numerous clayey-peaty lenses.

The convenience and good reliability of the present approach to estimate the spatial salinization patterns in coastal aquifers is promising for future research perspective. For example, a 3D geostatistical model, applied to a sub-portion of the domain used in this work's application, would reveal other insights about salinization in this area.

## Fundings

This research received no fundings.

## Software

All computations have been performed via GSLIB libraries (Deutsch and Journel, 1997) and an institutional Matlab license.

## CRediT authorship contribution statement

**Massimiliano Schiavo:** Conceptualization, Methodology, Formal analysis, Investigation, Data curation, Writing – original draft, Visualization. **Nicolò Colombani:** Conceptualization, Methodology, Validation, Formal analysis, Data curation, Writing – review & editing. **Micòl Mastrocicco:** Conceptualization, Validation, Investigation, Writing – review & editing, Supervision.

## Declaration of Competing Interest

The authors declare that they have no known competing financial

interests or personal relationships that could have appeared to influence the work reported in this paper.

## Data availability

Data will be made available on request.

## References

- Abu Al Naeem, M.F., Yusoff, I., Ng, T.F., Alias, Y., Raksmei, M., 2018. Assessment of groundwater salinity and quality in Gaza coastal aquifer, Gaza Strip, Palestine: an integrated statistical, geostatistical and hydrogeochemical approaches study. *Sci. Total Environ.* 615, 972–989. <https://doi.org/10.1016/j.scitotenv.2017.09.320>.
- Aiello, G., Barra, D., Collina, C., Piperno, M., Guidi, A., Stanislao, C., Saracino, M., Donadio, C., 2018. Geomorphological and paleoenvironmental evolution in the prehistoric framework of the coastland of Mondragone, southern Italy. *Quat. Int.* 493, 70–85. <https://doi.org/10.1016/j.quaint.2018.06.041>.
- Alagha, J.S., Seyam, M., Said, M.A.M., Mogheir, T., 2017. Integrating an artificial intelligence approach with k-means clustering to model groundwater salinity: the case of the Gaza coastal aquifer (Palestine). *Hydrogeol. J.* 25, 2347–2361. <https://doi.org/10.1007/s10040-017-1658-1>.
- Amorosi, A., Pacifico, A., Rossi, V., Ruberti, D., 2012. Late quaternary incision and deposition in an active volcanic setting: the Volturno valley fill, Southern Italy. *Sedim. Geol.* 282, 307–320. <https://doi.org/10.1016/j.sedgeo.2012.10.003>.
- Athens, N., Caers, J., 2022. Stochastic inversion of gravity data accounting for geological uncertainty. *Math. Geosci.* 54, 413–436. <https://doi.org/10.1007/s11004-021-09978-2>.
- Banusch, S., Somogyvári, M., Sauter, M., Renard, P., Engelhardt, I., 2022. Stochastic modeling approach to identify uncertainties of karst conduit networks in carbonate aquifers. *Water Resour. Res.* 58, e2021WR031710 <https://doi.org/10.1029/2021WR031710>.
- Barlow, P.M., 2003. Occurrence and flow of freshwater and saltwater in coastal aquifers. Barlow, P.M., Ed. *Ground Water in Freshwater-Saltwater Environments of the Atlantic Coast*. U.S. Geological Survey. <https://doi.org/10.3133/cir1262>. Reston, Chapter 1.
- Bauer, J., Börsig, N., Pham, V.C., Hoan, T.V., Nguyen, H.T., Norra, S., 2022. Geochemistry and evolution of groundwater resources in the context of salinization and freshening in the southernmost Mekong Delta, Vietnam. *J. Hydrol. Reg. Stud.* 40, 101010 <https://doi.org/10.1016/j.ejrh.2022.101010>.
- Bear, J., Cheng, A., Sorek, S., Ouazar, D., Herrera, I., 1999. *Seawater Intrusion in Coastal Aquifers - Concepts, Methods, and Practices. Theory and Applications of Transport in Porous Media*. Kluwer Academic Publishers.
- Beebe, C.R., Ferguson, G., Gleeson, T., Morgan, L.K., Werner, A., 2016. Application of an analytical solution as a screening tool for sea water intrusion. *Groundwater* 54 (5), 709–718. <https://doi.org/10.1111/gwat.12411>.
- Bierkens, M.F., Wada, Y., 2019. Non-renewable groundwater use and groundwater depletion: a review. *Environ. Res. Lett.* 14 (6), 063002 <https://doi.org/10.1088/1748-9326/ab1a5f>.
- Busico, G., Buffardi, C., Ntona, M.M., Vigliotti, M., Colombani, N., Mastrocicco, M., Ruberti, D., 2021. Actual and forecasted vulnerability assessment to seawater intrusion via GALDIT\_SUSI in the Volturno river mouth (Italy). *Remote Sens.* 13 (18), 3632. <https://doi.org/10.3390/rs13183632>.
- Carol, E.S., Del Pilar Alvarez, M., Tanjal, C., Bouza, P.J., 2021a. Factors controlling groundwater salinization processes in coastal aquifers in semiarid environments of north Patagonia, Argentina. *J. South Am. Earth Sci.* 110, 103356 <https://doi.org/10.1016/j.jsames.2021.103356>.
- Carol, E.S., Perdomo, S., Alvarez, M.d.P., Tanjal, C., Bouza, P., 2021b. Hydrochemical, isotopic, and geophysical studies applied to the evaluation of groundwater salinization processes in quaternary beach ridges in a semiarid coastal area of northern Patagonia, Argentina. *Water* 13 (24), 3509. <https://doi.org/10.3390/w13243509>.
- Cary, L., Petelet, G.E., Bertrand, G., Kloppmann, W., Aquilina, L., Martins, V., Hirata, R., Montenegro, S., Pauwels, H., Chatton, E., Franzen, M., Aurouet, A., Lasseur, E., Picot, G., Guerrot, C., Fléhoc, C., Labasque, T., Santos, J.G., Paiva, A., Braibant, G., Pierre, D., 2015. Origins and processes of groundwater salinization in the urban coastal aquifers of Recife (Pernambuco, Brazil): a multi-isotope approach. *Sci. Total Environ.* 530–531, 411–429. <https://doi.org/10.1016/j.scitotenv.2015.05.015>.
- Caschetto, M., Colombani, N., Mastrocicco, M., Petitta, M., Aravena, R., 2017. Nitrogen and sulphur cycling in the saline coastal aquifer of Ferrara, Italy. A multi-isotope approach. *Appl. Geochem.* 76, 88–98. <https://doi.org/10.1016/j.apgeochem.2016.11.014>.
- Chiles, J.P., Delfiner, P., 2009. *Geostatistics: Modeling Spatial Uncertainty* (Vol. 497). John Wiley & Sons, ISBN: 978-0-470-18315-1.
- Comte, J.C., Banton, O., 2007. Cross-validation of geo-electrical and hydrogeological models to evaluate seawater intrusion in coastal aquifers. *Geophys. Res. Lett.* 34 (10), L10402. <https://doi.org/10.1029/2007GL029981>.
- Cornielio, A., Ducci, D., 2014. Hydrogeochemical characterization of the main aquifer of the "Litorale Domizio-Agro Aversano NIPS" (Campania-southern Italy). *J. Geochem. Explor.* 137, 1–10. <https://doi.org/10.1016/j.jgexplo.2013.10.016>.
- Custodio, E., 1988. Present state of coastal aquifer modelling: short review. Custodio, E., Gurgui, A., Ferreira, J.P.L. (eds). *Groundwater Flow and Quality Modelling*. NATO



- ASI Series, vol. 224. Springer, Dordrecht. [https://doi.org/10.1007/978-94-009-2889-3\\_40](https://doi.org/10.1007/978-94-009-2889-3_40).
- De Franco, R., Biella, G., Tosi, L., Teatini, P., Lozej, A., Chiozzotto, B., Giada, M., Rizzetto, F., Claude, C., Mayer, A., Bassan, V., Gasparetto-Stori, G., 2009. Monitoring the saltwater intrusion by time lapse electrical resistivity tomography: the Chioggia test site (Venice Lagoon, Italy). *J. Appl. Geophys.* 69 (3–4), 117–130. <https://doi.org/10.1016/j.jappgeo.2009.08.004>.
- De Montety, V., Radakovitch, O., Vallet-Coulomb, C., Blavoux, B., Hermitte, D., Valles, V., 2008. Origin of groundwater salinity and hydrogeochemical processes in a confined coastal aquifer: case of the Rhone delta (Southern France). *Appl. Geochem.* 23 (8), 2337–2349. <https://doi.org/10.1016/j.apgeochem.2008.03.011>.
- Delsman, J.R., Hu-a-ng, K.R.M., Vos, P.C., de Louw, P.G.B., Oude Essink, G.H.P., Stuyfzand, P.J., Bierkens, M.F.P., 2014. Paleo-modeling of coastal saltwater intrusion during the Holocene: an application to the Netherlands. *Hydrol. Earth Syst. Sci.* 18, 3891–3905. <https://doi.org/10.5194/hess-18-3891-2014>.
- Deutsch, C.V., Journel, A., 1997. *Geostatistical Software Library and User's Guide*. Oxford University Press, New York.
- Fiori, A., Bellin, A., Cvetkovic, V., de Barros, F., Dagan, G., 2015. Stochastic modeling of solute transport in aquifers: from heterogeneity characterization to risk analysis. *Water Resour. Res.* 51, 6622–6648. <https://doi.org/10.1002/2015WR017388>.
- Gaiolini, M., Colombani, N., Busico, G., Rama, F., Mastrocicco, M., 2022. Impact of boundary conditions dynamics on groundwater budget in the Campania region (Italy). *Water* 14 (16), 2462. <https://doi.org/10.3390/w14162462>.
- Goovaerts, P., 1997. *Geostatistics for Natural Resources Evaluation*. Oxford University Press, New York.
- Isaaks, E.H., Srivastava, R.M., 1989. *Applied Geostatistics*. Oxford University press, New York.
- Jamei, M., Karbasi, M., Malik, A., Abualigah, L., Islam, A.R.M.T., Yaseen, Z.M., 2022. Computational assessment of groundwater salinity distribution within coastal multi-aquifers of Bangladesh. *Sci. Rep.* 12 (1), 11165. <https://doi.org/10.1038/s41598-022-15104-x>.
- Katerji, N., Van Hoorn, J.W., Hamdy, A., Mastrocicco, M., 2003. Salinity effect on crop development and yield, analysis of salt tolerance according to several classification methods. *Agric. Water Manage.* 62 (1), 37–66. [https://doi.org/10.1016/S0378-3774\(03\)00005-2](https://doi.org/10.1016/S0378-3774(03)00005-2).
- Kazakis, N., Busico, G., Colombani, N., Mastrocicco, M., Pavlou, A., Voudouris, K., 2019. GALDIT-SUSI a modified method to account for surface water bodies in the assessment of aquifer vulnerability to seawater intrusion. *J. Environ. Manage.* 235, 257–265. <https://doi.org/10.1016/j.jenvman.2019.01.069>.
- Kim, K.Y., Chon, C.M., Park, K.H., 2007. A simple method for locating the fresh water-salt water interface using pressure data. *Ground Water* 45 (6), 723–738. <https://doi.org/10.1111/j.1745-6584.2007.00349.x>.
- Klassen, J., Allen, D.M., 2017. Assessing the risk of saltwater intrusion in coastal aquifers. *J. Hydrol.* 551, 730–745. <https://doi.org/10.1016/j.jhydrol.2017.02.044>.
- Koukadaki, M.A., Karatzas, G.P., Papadopolou, M.P., Vafidis, A., 2007. Identification of the saline zone in a coastal aquifer using electrical tomography data and simulation. *Water Resour. Manage.* 21 (11), 1881–1898. <https://doi.org/10.1007/s11269-006-9135-y>.
- Langevin, C.D., Thorne Jr., D.T., Dausman, A.M., Sukop, M.C., Guo, W., 2007. SEAWAT Version 4: A Computer Program for Simulation of Multi-Species Solute and Heat Transport. U.S. Geol. Surv. Tech. Methods. <https://doi.org/10.3133/tm6A22>. Book 6, Chapter A22, 39 p.
- Liu, S., Tang, Z., Gao, M., Hou, G., 2017. Evolutionary process of saline-water intrusion in Holocene and Late Pleistocene groundwater in southern Laizhou Bay. *Sci. Total Environ.* 607, 586–599. <https://doi.org/10.1016/j.scitotenv.2017.06.262>.
- Mastrocicco, M., Busico, G., Colombani, N., Vigliotti, M., Ruberti, D., 2019. Modelling actual and future seawater intrusion in the Variconi coastal wetland (Italy) due to climate and landscape changes. *Water* 11 (7), 1502. <https://doi.org/10.3390/w11071502>.
- Mastrocicco, M., Colombani, M., 2021. The issue of groundwater salinization in coastal areas of the Mediterranean region: a review. *Water* 13 (1), 90. <https://doi.org/10.3390/w13010090>.
- Mastrocicco, M., Gervasio, M.P., Busico, G., Colombani, N., 2021. Natural and anthropogenic factors driving groundwater resources salinization for agriculture use in the Campania plains (Southern Italy). *Sci. Total Environ.* 758, 144033. <https://doi.org/10.1016/j.scitotenv.2020.144033>.
- Matano, F., Critelli, S., Barone, M., Muto, F., Di Nocera, S., 2014. Stratigraphic and provenance evolution of the Southern Apennines foreland basin system during the Middle Miocene to Pliocene (Irpina-Sannio successions, Italy). *Mar. Petr. Geol.* 57, 652–670. <https://doi.org/10.1016/j.marpetgeo.2014.07.012>.
- Matano, F., Sacchi, M., Vigliotti, M., Ruberti, D., 2018. Subsidence trends of Volturno river Coastal plain (Northern Campania, Southern Italy) inferred by SAR interferometry data. *Geosciences* 8 (1), 8. <https://doi.org/10.3390/geosciences8010008>.
- Meyer, R., Engesgaard, P., Sonnenborg, T.O., 2019. Origin and dynamics of saltwater intrusion in a regional aquifer: combining 3-D saltwater modeling with geophysical and geochemical data. *Water Resour. Res.* 55 (3), 1792–1813. <https://doi.org/10.1029/2018WR023624>.
- Motavalli, A., Naghibi, S.A., Hashemi, H., Berndtsson, R., Pradham, Gholami, V., 2019. Inverse method using boosted regression tree and k-nearest neighbor to quantify effects of point and non-point source nitrate pollution in groundwater. *J. Clean. Prod.* 228, 1248–1263. <https://doi.org/10.1016/j.jclepro.2019.04.293>.
- Nash, J.E., Sutcliffe, J.V., 1970. River flow forecasting through conceptual models part I. A discussion of principles. *J. Hydrol.* 10 (3), 282–290. [https://doi.org/10.1016/0022-1694\(70\)90255-6](https://doi.org/10.1016/0022-1694(70)90255-6).
- Panagiotou, C.F., Tziritis, E., Kyriakidis, P., 2022. Application of geostatistical methods to groundwater salinization problems: a review. *J. Hydrol.* 128566. <https://doi.org/10.1016/j.jhydrol.2022.128566>.
- Pool, M., Carrera, J., Alcolea, A., Bocanegra, E.M., 2015. A comparison of deterministic and stochastic approaches for regional scale inverse modeling on the Mar del Plata aquifer. *J. Hydrol.* 531, 214–229. <https://doi.org/10.1016/j.jhydrol.2015.09.064>.
- Rasmussen, P., Sonnenborg, T.O., Gonciar, G., Hinsby, K., 2013. Assessing impacts of climate change, sea level rise, and drainage canals on saltwater intrusion to coastal aquifer. *Hydrol. Earth Syst. Sci.* 17, 421–443. <https://doi.org/10.5194/hess-17-421-2013>.
- Ruberti, D., Buffardi, C., Sacchi, M., Vigliotti, M., 2022. The late Pleistocene-Holocene changing morphology of the Volturno delta and coast (northern Campania, Italy): Geological architecture and human influence. *Quat. Inter.* 625, 14–28. <https://doi.org/10.1016/j.quaint.2022.03.023>.
- Sacchi, M., Molisso, F., Pacifico, A., Vigliotti, M., Sabbarese, C., Ruberti, D., 2014. Late-Holocene to recent evolution of Lake Patria, South Italy: an example of a coastal lagoon within a Mediterranean delta system. *Glob. Planet. Change* 117, 9–27. <https://doi.org/10.1016/j.gloplacha.2014.03.004>.
- Sanchez-Vila, X., Fernandez-Garcia, D., 2016. Debates—Stochastic subsurface hydrology from theory to practice: Why stochastic modeling has not yet permeated into practitioners? *Water Resour. Res.* 52 (12), 9246–9258. <https://doi.org/10.1002/2016WR019302>.
- Schiavo, M., 2022a. Probabilistic delineation of subsurface pathways in alluvial aquifers under geological uncertainty. *J. Hydrol.* 614, 128674. <https://doi.org/10.1016/j.jhydrol.2022.128674>.
- Schiavo, M., 2022b. The role of different sources of uncertainty on the stochastic quantification of subsurface discharges in heterogeneous aquifers. *J. Hydrol.* 617, 128930. <https://doi.org/10.1016/j.jhydrol.2022.128930>.
- Schiavo, M., Riva, M., Guadagnini, L., Zehe, E., Guadagnini, A., 2022. Probabilistic identification of preferential groundwater networks. *J. Hydrol.* 610, 127906. <https://doi.org/10.1016/j.jhydrol.2022.127906>.
- Taşan, M., Taşan, S., Demir, Y., 2022. Estimation and uncertainty analysis of groundwater quality parameters in a coastal aquifer under seawater intrusion: a comparative study of deep learning and classic machine learning methods. *Environ. Sci. Pollut. Res.* 1–25. <https://doi.org/10.1007/s11356-022-22375-4>.
- Taylor, J.R., 1997. *An Introduction to Error Analysis: The study of uncertainties in physical measurements* (2nd ed.). University Science Books. P. 217, Sausalito, CA. ISBN 0-935702-75-X.
- Tomaszkiewicz, M., Abou Najm, M., El-Fadel, M., 2014. Development of a groundwater quality index for seawater intrusion in coastal aquifers. *Environ. Mod. Soft.* 57, 13–26. <https://doi.org/10.1016/j.envsoft.2014.03.010>.
- Trabelsi, F., Ben Mammou, A., Tarhouni, J., Piga, C., Ranieri, G., 2013. Delineation of saltwater intrusion zones using the time domain electromagnetic method: the Nabeul-Hammamet coastal aquifer case study (NE Tunisia). *Hydrol. Process.* 27, 2004–2020. <https://doi.org/10.1002/hyp.9354>.
- Trabelsi, N., Triki, I., Hentati, I., Zairi, M., 2016. Aquifer vulnerability and seawater intrusion risk using GALDIT, GQISWI and GIS: case of a coastal aquifer in Tunisia. *Environ. Earth Sci.* 75, 669. <https://doi.org/10.1007/s12665-016-5459-y>.
- Trichakis, I.C., Nikolos, I., Karatzas, G., 2011. Artificial neural network (ANN) based modeling for karstic groundwater level simulation. *Water Resour. Manage.* 25 (4), 1143–1152. <https://doi.org/10.1007/s11269-010-9628-6>.
- Wang, Y., Jiao, J.J., 2012. Origin of groundwater salinity and hydrogeochemical processes in the confined Quaternary aquifer of the Pearl River Delta. *China. J. Hydrol.* 438–439, 112–124. <https://doi.org/10.1016/j.jhydrol.2012.03.008>.
- Werner, A.D., Bakker, M., Post, V.E.A., Vandenbohede, A., Lu, C., Ataie-Ashtiani, B., Simmons, C.T., Barry, D.A., 2013. Seawater intrusion processes, investigation and management: recent advances and future challenges. *Adv. Wat. Res.* 51, 3–26. <https://doi.org/10.1016/j.advwatres.2012.03.004>.
- Zanchetta, G., Sulpizio, R., Di Vito, M.A., 2004. The role of volcanic activity and climate in alluvial fan growth at volcanic areas: an example from southern Campania (Italy). *Sedim. Geol.* 168, 249–280. <https://doi.org/10.1016/j.sedgeo.2004.04.001>.
- Zhao, Q., Su, X., Kang, B., Zhang, Y., Wu, X., Liu, M., 2017. A hydrogeochemistry and multi-isotope (Sr, O, H, and C) study of groundwater salinity origin and hydrogeochemical processes in the shallow confined aquifer of northern Yangtze River downstream coastal plain, China. *Appl. Geochem.* 86, 49–58. <https://doi.org/10.1016/j.apgeochem.2017.09.015>.